Antiviral Research 162 (2019) 178–185

Contents lists available at ScienceDirect

Antiviral Research

journal homepage: www.elsevier.com/locate/antiviral

Mutation and structure guided discovery of an antiviral small molecule that mimics an essential C-Terminal tripeptide of the vaccinia D4 processivity factor

Manunya Nuth[a], Hancheng Guan[a], Yuhong Xiao[c], John L. Kulp III[d], Michael H. Parker[e], Eric D. Strobel[e], Stuart N. Isaacs[c], Richard W. Scott[e], Allen B. Reitz[e], Robert P. Ricciardi[a,b,*]

[a] Department of Microbiology, School of Dental Medicine and the Abramson Cancer Center, Perelman School of Medicine, University of Pennsylvania, Philadelphia, PA, USA
[b] Abramson Cancer Center, Perelman School of Medicine, University of Pennsylvania, Philadelphia, PA, USA
[c] Department of Medicine, Division of Infectious Diseases, Perelman School of Medicine, University of Pennsylvania, Philadelphia, PA, USA
[d] Conifer Point Pharmaceuticals, Doylestown, PA, USA
[e] Fox Chase Chemical Diversity Center, Inc., Doylestown, PA, USA

ARTICLE INFO

Keywords:
Antiviral
Drug design
DNA synthesis
Poxvirus
Processivity

ABSTRACT

The smallpox virus (variola) remains a bioterrorism threat since a majority of the human population has never been vaccinated. In the event of an outbreak, at least two drugs against different targets of variola are critical to circumvent potential viral mutants that acquire resistance. Vaccinia virus (VACV) is the model virus used in the laboratory for studying smallpox. The VACV processivity factor D4 is an ideal therapeutic target since it is both essential and specific for poxvirus replication. Recently, we identified a tripeptide (Gly-Phe-Ile) motif at the C-terminus of D4 that is conserved among poxviruses and is necessary for maintaining protein function. In the current work, a virtual screening for small molecule mimics of the tripeptide identified a thiophene lead that effectively inhibited VACV, cowpox virus, and rabbitpox virus in cell culture (EC_{50} = 8.4–19.7 μM) and blocked *in vitro* processive DNA synthesis (IC_{50} = 13.4 μM). Compound-binding to D4 was demonstrated through various biophysical methods and a dose-dependent retardation of the proteolysis of D4 proteins. This study highlights an inhibitor design strategy that exploits a susceptible region of the protein and identifies a novel scaffold for a broad-spectrum poxvirus inhibitor.

1. Introduction

Smallpox is an infectious disease caused by variola virus that has killed hundreds of millions of people throughout history. Although globally eradicated in 1980 (Fenner et al., 1988), it poses a modern-day bioterrorism threat for the majority of the current population who remain unvaccinated (Longini et al., 2007). Indeed, smallpox poses a national security risk and is considered a Category A (highest priority) agent by the Centers for Disease Control and Prevention. Tecovirimat (also known as ST-246 and under the brand name, TPOXX, SIGA Technologies Inc.) (Grosenbach et al., 2018) was recently approved by the Food and Drug Administration for the treatment of smallpox. With the potential of poxvirus variants to develop resistance either through single-agent treatment or intentional engineering, it is important to develop a second therapeutic that will recognize a completely different viral target. The combination of tecovirimat and the new therapeutic could serve to circumvent both the natural and intentional generation of drug resistant variola.

Vaccinia virus (VACV) is a prototypic orthopoxvirus and the laboratory model for studying smallpox. Orthopoxviruses are highly conserved, sharing > 90% nucleotide identity (Gubser et al., 2004), with the laboratory VACV-WR strain used for this study possessing 96% nucleotide identity to variola (Aguado et al., 1992). The poxvirus processivity factor comprises two essential proteins – A20 and D4 – that

Abbreviations: CDV, cidofovir; CPXV, cowpox virus; EtBr, ethidium bromide; DTT, dithiothreitol; DMSO, dimethyl sulfoxide; FPLC, fast protein column chromatography; hERβ-N, human estrogen receptor beta; IPTG, isopropyl β-D-1-thiogalactopyranoside; ITC, isothermal titration calorimetry; MBP, maltose binding protein; MD, molecular dynamics; NTA, nitrilotriacetic acid; RPXV, rabbitpox virus; SPR, surface plasmon resonance; ssDNA, single-stranded DNA; VACV, vaccinia virus

* Corresponding author. Department of Microbiology, School of Dental Medicine and the Abramson Cancer Center, Perelman School of Medicine, University of Pennsylvania, Philadelphia, PA, USA.
E-mail address: Ricciard@upenn.edu (R.P. Ricciardi).

https://doi.org/10.1016/j.antiviral.2018.12.011
Received 22 October 2018; Received in revised form 12 December 2018; Accepted 17 December 2018
Available online 20 December 2018
0166-3542/

help its cognate DNA polymerase synthesize extended DNA strands (Czarnecki and Traktman, 2017). Since processivity factors are specific for their cognate DNA polymerases (Ellison and Stillman, 2001), D4 serves as a compelling therapeutic target to block poxvirus replication. D4 is conserved among all poxviruses (Dabrowski et al., 2013), possessing 99% protein sequence similarity to variola (Supplementary Fig. S1). VACV D4 is a 25-kDa protein with a dual-function required for DNA repair (as a uracil-DNA glycosylase) and processive DNA synthesis (Boyle et al., 2011; Druck Shudofsky et al., 2010; Millns et al., 1994; Stuart et al., 1993; Upton et al., 1993). As such, it is capable of binding to DNA. VACV A20 is a 49-kDa protein that binds D4 and DNA polymerase, thus allowing the DNA-scanning action of D4 to tether the DNA polymerase onto the DNA template and enabling it to synthesize extended strands without dissociating from the DNA (Stanitsa et al., 2006).

In previous studies, we performed chemical library screening to identify small molecules with therapeutic potential for blocking VACV infection by targeting viral processivity (Ciustea et al., 2008; Nuth et al., 2011, 2013; Schormann et al., 2011; Silverman et al., 2008). Our most recent study revealed that the extreme C-terminus of D4 is required for maintaining protein integrity and function, with a tripeptide comprised of ^{215}Gly-Phe-Ile^{217}, which is adjacent to a predicted region of protein disorder, playing an important role (Nuth et al., 2016). Since disorder is a reflection of protein dynamics, and that dynamics _EN-REF_20governs protein function and molecular recognition (Gibbs, 2014), we speculated that the perturbation of the tripeptide could interfere with D4 function by disrupting the dynamics (Nuth et al., 2016). In the current work, we exploit the susceptibility of the C-terminus as the basis for an inhibitor design by targeting the tripeptide.

2. Materials and methods

2.1. Compounds

Compounds were purchased from MolPort (Latvia) and were comprised of compounds procured from various vendors as listed in Supplementary Table S1. Cidofovir was purchased from Selleck Chemicals, and tecovirimat was prepared by the method of Bailey et al. (2007). All compounds were declared > 95% pure by the vendors and used as 10 mM solutions in DMSO.

2.2. Virtual screening for ^{215}GFI^{217} small molecule mimics and compound selection

The crystal structure of D4 was uploaded as a PDB file (PDB ID: 4ODA) onto the web interface of pepMMsMIMIC (Floris et al., 2011), and the ^{215}GFI^{217}sequence of chain A was selected as the region for query. Two lists, containing 200 compounds per list, were compiled on the basis of shape similarity and shape/pharmacophore. The removal of pan assay interference compounds (PAINS) (Baell and Holloway, 2010) and further binning using a Tanimoto coefficient of 0.9 allowed grouping of conformers and chemically-similar compounds. Twenty chemically-diverse compounds were chosen on the basis of rank-order designated by pepMMsMIMIC and commercial availability. The 20 compounds were subsequently screened at a single dose of 50 μM for the ability to inhibit VACV infection in plaque reduction assays. Compounds that showed ≥50% inhibition were subjected to dose-response studies in plaque reduction assays and *in vitro* processive DNA synthesis.

2.3. Molecular dynamics and molecular docking

Simulation steps were carried out with the Amber99SB force field (Hornak et al., 2006) within the GROMACS software package (Pronk et al., 2013). Hydrogens were added and optimized with the protein preparation module in Schrödinger Inc. software (Sastry et al., 2013). The simulation was run in a cubic box with a 1.0 Å distance between the solute and the box, and the system was solvated with water model (spc216.gro) with 150 mM NaCl ions in the box. After the removal of all other chains, chain A of D4 (PDB ID: 4ODA) was energy minimized with 1000 steps using steepest descent algorithm and periodically subjecting the systems to a conjugant gradient algorithm once every 10 steps. Prior to production dynamics, 100 ps of restrained dynamics was run to relax the water in the system while applying restraints to the protein. The MD simulation was run for 5,000,000 steps (10 ns).

The procedure for docking of FC-6407 onto D4 was similar to the previously described method (Nuth et al., 2013) using chain A of D4 (PDB ID: 4ODA) removed of the C-terminal six residues ^{213}AQGFIY^{218} as to permit access by the compound.

2.4. Protein production

His- (His_6D4 and MBP-His_8) and MBP-tagged (MBP-$A20_{63}$) proteins were constructed, expressed in Rosetta2pLysS, purified by Ni-NTA resins and gel filtration column chromatography, and handled as before (Nuth et al., 2016). Unless noted, the N-terminal His-tag of D4 proteins were removed by TEV protease (Nuth et al., 2016) and maintained in the eluting column buffer: 20 mM sodium phosphate (pH 6.8), 200 mM NaCl, and 15% w/v glycerol. The corresponding DNA sequence of the N-terminal 103-aa of the human estrogen receptor beta (hERβ-N) (Warnmark et al., 2001) was obtained as a codon-optimized synthetic gene (Integrated DNA Technologies, Inc.) and inserted into the pMAL-c2X vector (New England Biolabs, Inc.) at the *Eco*RI and *Hin*dIII sites in order to generate a fusion protein C-terminal to MBP.

2.5. Drug affinity responsive target stability (DARTS)

Experiments were adapted from Lomenick et al. (2009) using bacterial cell lysates. Rosetta2pLysS cells harboring the constructs of interest were induced with 0.2 mM isopropyl β-D-1-thiogalactopyranoside overnight at room temperature, and 3–5 mL of the cell suspension was pelleted and used for an experiment. Cells pellets were resuspended in 500 μL of 20 mM sodium phosphate (pH 6.8), 200 M NaCl, and 0.5% w/v Triton X-100 and lysed by five pulses of 5-s ultrasonication. After 5-min centrifugation at 15,000 rpm, the cleared lysate was diluted 40-fold into 100 μL reaction volume of the same buffer absence the Triton X-100 but with added 2.5 mM DTT, 1% DMSO, and 0.005% Tween-20, thus giving an effective Triton X-100 concentration ~0.012%. Proteolysis was achieved with the addition of 5 μL Pronase (Calbiochem; prepared as 10 mg/mL stock in 50 mM Tris (pH 8) and 40 mM $CaCl_2$) and incubation at 30 °C for 30 min. For compound-binding studies, the diluted lysates were combined with 2-fold serial dilutions of compounds, incubated for 30 min at 25 °C, and followed by the Pronase digestion. Reactions were stopped with the addition of 20 μL of 5X SDS-PAGE loading buffer and heated at 90 °C for 5 min. Fifteen microliter of the mix was loaded onto a 4–12% Bis-Tris mini gel, and Western blot was performed under standard protocol by probing proteins with 1:1000 anti-His (GE Healthcare Life Sciences) or 1:2000 anti-MBP (New England Biolabs, Inc.) antibody.

2.6. Maleimide dye conjugation

Cysteine substitutions were introduced by site-directed mutagenesis at positions −19 (-G19C; 19-aa upstream of Met of D4 and immediately after the AUG start codon) and 219 (Δ219C; with a stop codon following Cys^{219}) to permit conjugation to fluorescein-5-maleimide (AnaSpec Inc.) or N-(1-pyrene)maleimide (ThermoFisher Scientific). Dye stocks were prepared at 10 mg/mL in DMSO. Prior to the gel filtration step of protein purification, proteins were treated with 10 mM DTT for 30 min at room temperature. Protein eluates were maintained at < 25 μM concentrations and immediately added with four molar equivalents of dyes in column buffer containing 0.01% Triton X-100 and 5 mM EDTA and left overnight at 4 °C away from light. The protein/

dye mixes were then centrifuged to remove particulates and the supernatants passed twice through Bio-Beads SM2 resins (Bio-Rad) to remove Triton X-100. The eluates were further concentrated and purified by gel filtration to remove unbound dyes, EDTA, and salts. Both purified proteins were further confirmed by their fluorescence properties: 343 nm excitation/375 nm emission for pyrene and 493/517 nm for fluorescein (data not shown).

2.7. Data manipulation and presentation

All plots and curve-fitting were processed by Prism 5.0 (GraphPad Software, Inc.) and protein images depicted with UCSF Chimera (Pettersen et al., 2004).

3. Results

3.1. Supports for protein dynamics of D4

Previous findings suggested protein dynamics to play an important role in the function of D4 (Nuth et al., 2016). Therefore, the disruption of this dynamics could be an effective strategy for inhibitor design. Accordingly, the examination of the intrinsic fluorescence of D4 in the presence of 0.5–5% DMSO showed pronounced decrease in emission (Fig. 1A). Given that tryptophan quenching is mediated through a solvent-stabilized charge-transfer of the ring-to-peptide backbone (Cowgill, 1970; Muino and Callis, 2009), the observed fluctuation in fluorescence is in line with the DMSO − H_2O exchange at the protein surface, which could conceivably be accelerated by a dynamic protein. By comparison, the well-folded maltose binding protein (MBP) lacked a similar trend (Fig. 1A).

Next, we examined the protease sensitivity of test proteins, since it is established that unfolded or partially-folded proteins are more prone to proteolysis than those that are well-structured (Wright and Dyson, 1999). Bacterial lysates expressing recombinant proteins of various degrees of protein folding were exposed to the nonspecific protease, Pronase, according to the drug affinity responsive target stability (DARTS) (Lomenick et al., 2009) protocol and then probed by Western blot. As expected, MBP was the most resistant to proteolysis compared to the other tested proteins even at 1:37.5 Pronase dilution (equivalent to 12.7 μg/mL of protease), while D4 was largely undetected at the tested 1:150 Pronase dilution (Fig. 1B). In order to contrast the levels of protease sensitivity relative to MBP, two proteins with known or speculated dynamics were examined. The N-terminal 103-aa of human estrogen receptor beta (hERβ-N), which, in the absence of a carrier protein, is expressed as an inclusion body that can be refolded *in vitro* into an intrinsically disordered structure (Warnmark et al., 2001). As an MBP fusion, hERβ-N was detected as a minor product in the crude lysate that showed strong susceptibility to proteolysis even down to 1:1200 Pronase dilution (Fig. 1B). Likewise, MBP fusion of the N-terminal 63-amino acid portion of A20 rendered the fusion protein more susceptible to proteolysis than MBP alone, with protein levels largely undetected at 1:75 Pronase dilution (Fig. 1B), an observation in agreement with the speculated disordered/unfolded state of the 63-amino acid peptide prior to binding D4 (Nuth et al., 2016). Taken together, the solvent exposure and DARTS results provided consistent demonstration of protein dynamics and showed D4 neither exhibited properties equivalent to a well-folded protein such as MBP nor that with defined disorder. Thus, dynamics could likely originate from local regions, with the C-terminus of the protein as one likely source.

3.2. Targeting the C-terminus of D4 for inhibitor design

As we previously showed, protein perturbation was more pronounced when alterations were made at the C-terminus of D4 as compared to the N-terminus (Nuth et al., 2016). In order to simulate the impact of perturbation by small molecules on the protein's termini, we compared how the covalent attachment of dyes at either the N- or C-terminus of D4 would affect the protein recovery after the conjugation reaction. Because purified proteins were used, the rationale was that any loss of soluble proteins would be directly caused by the dye. From the crystal structure of D4 (PDB ID: 4ODA), none of its natural four cysteine residues are solvent-accessible (data not shown). Thus, a solvent-accessible cysteine was introduced by mutagenesis at either the protein's N-terminus, 19 amino acids beyond D4's starting methionine

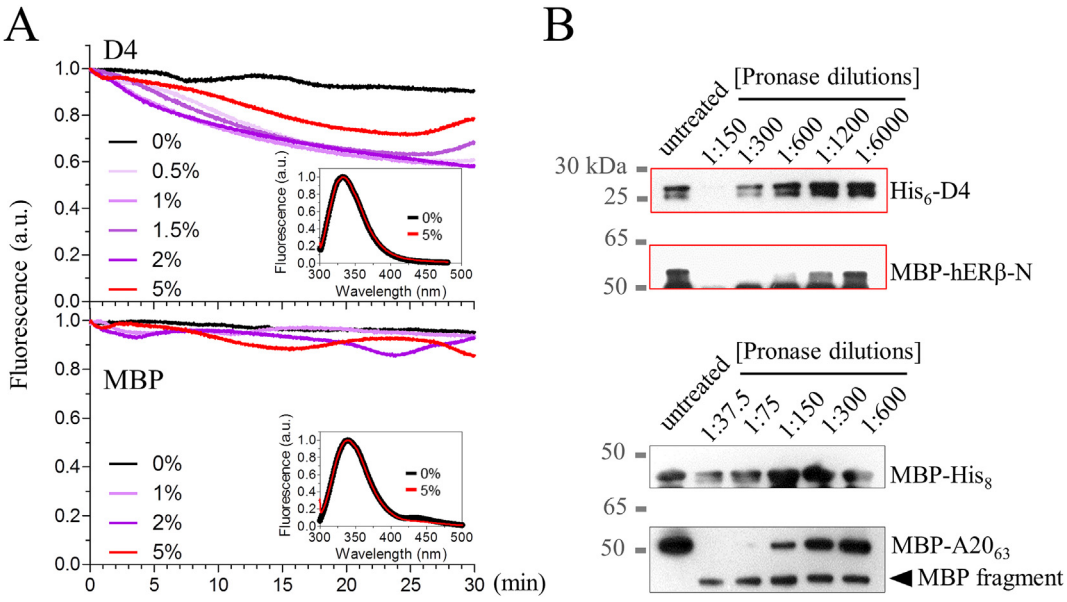

Fig. 1. Protein dynamics is exhibited by the D4 protein. (A) Tryptophan emission profiles of D4 and MBP are shown in the presence of the indicated concentrations of DMSO. The difference spectra at 0 and 5% DMSO for both proteins suggest no disruption to overall protein folding (insets). (B) Protease sensitivity. Pronase was prepared as a 10 mg/mL stock and diluted as indicated. Proteins are depicted with their corresponding tags in order to permit probing by the appropriate antibodies during Western blot. His-tagged D4 (~27 kDa) was probed with anti-His antibody, while MBP fusions of human estrogen receptor beta (hERβ-N; ~54 kDa), MBP (introduced with a C-terminal His_8; ~44 kDa), and the N-terminal 63-aa acid stretch of A20 ($A20_{63}$; ~52 kDa) were probed with anti-MBP antibody. The efficiency by which a protein is degraded by Pronase is compared to its untreated lane.

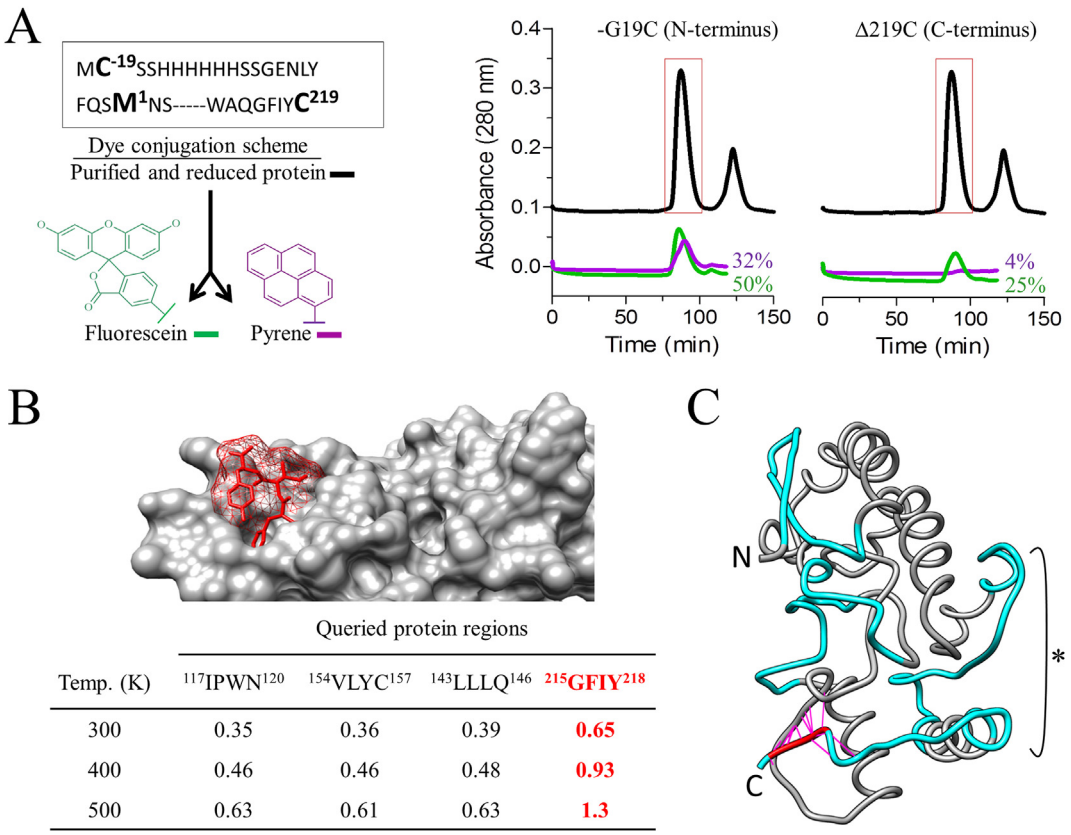

Queried protein regions

Temp. (K)	^{117}IPWN^{120}	^{154}VLYC^{157}	^{143}LLLQ^{146}	^{215}GFIY^{218}
300	0.35	0.36	0.39	**0.65**
400	0.46	0.46	0.48	**0.93**
500	0.63	0.61	0.63	**1.3**

Fig. 2. The C-terminus of D4 is a target for inhibitor design. (A) The impact of dye attachment at either the N- (-G19C mutation) or C-terminus (Δ219C mutation) of purified D4 proteins, with the corresponding N- and C-terminal sequences shown boxed. M^1 is D4's starting Met. Comparable protein amounts collected from Ni-NTA fractions were reduced with DTT and eluted by gel filtration on a fast protein liquid chromatography (FPLC). Each half of an eluted protein fraction was then alkylated with either a fluorescein or pyrene dye. Depicted are the FPLC chromatograms of proteins pre- (black) and post-conjugation (green and magenta), whereby the percentages of recovered proteins were estimated from the ratio of the maximum absorbance values of the pre- and post-conjugation fractions of collected D4 fractions. The column fractions corresponding to D4 are shown boxed, while the unboxed peaks correspond to low molecular weight salts and free dyes. (B) Accessibility of the C-terminus. Shown are the root-mean-square deviation values of the indicated peptide regions generated by 10 ns MD simulations, with the region of interest in red and comprising the ^{215}GFI^{217} tripeptide. (C) Displacement of ^{215}GFI^{217} (red) could promote protein misfolding. From the crystal structure of D4 (PDB ID: 4ODA), ^{215}GFI^{217} makes intramolecular contacts with residues I96, S97, V102, Y105, K106, G107, Y108, N109, I113, W212, A213, and Q214 (magenta). The five predicted regions of protein disorder (Nuth et al., 2016) are shown (cyan), with the overlapping and proximal regions to ^{215}GFI^{217} comprising parts of the binding interfaces for D4 – A20 or D4 – D4 indicated by the asterisk.

that corresponded to the penultimate glycine (-G19C) or the protein's stop codon (Δ219C) in order to permit cysteinyl alkylation with fluorescein and pyrene maleimide dyes. Importantly, the point mutations proved innocuous as both proteins retained the ability to function as processivity factors in the ELISA-based *in vitro* processive DNA synthesis assay (Ricciardi et al., 2005) (data not shown). As shown in Fig. 2A, the conjugation at Cys^{-19} with either dye led to demonstrable protein recoveries after the conjugation reaction and subsequent purification steps (32% for pyrene and 50% for fluorescein after the final gel filtration step). By contrast, the labeling of Cys^{219} with pyrene resulted in the dramatic loss of D4 recovery (4%, which likely reflected an overestimation), while fluorescein labeling resulted in only 25% protein recovery. Given that properly folded and functional proteins were used, the loss of soluble proteins would be consistent with the promotion of protein misfolding as earlier speculated (Nuth et al., 2016). Taking advantage of pyrene (MW ~ 200) and fluorescein (MW ~ 330) as reasonable mimics of small molecules, these results reinforced the notion that the disruption of the C-terminus would have a profound effect on protein perturbation. Pyrene was especially disruptive when conjugated at the C-terminus, with its planar and rigid properties in line with the introduction of unfavorable entropy onto a presumably conformationally dynamic region of the protein.

The ^{215}GFI^{217} tripeptide at the C-terminus of D4 provides key intramolecular contacts for the production of proteins that are functional in processive DNA synthesis (Nuth et al., 2016). Therefore, an inhibitor capable of disrupting the C-terminus of D4 would act as a competitor of the tripeptide. As such, we examined whether this region of the protein was accessible to inhibitor binding by examining the protein backbone movement by molecular dynamics (MD) simulation. The C-terminal ^{215}GFIY^{218} (whereby Tyr^{218} represented the last and dispensable residue in the D4 protein) (Nuth et al., 2016) was compared to three randomly-chosen buried regions within the protein's interior to serve as rigid sites. As shown in Fig. 2B for a 10 ns MD simulation, protein movement was observed for ^{215}GFIY^{218} compared to the three reference sites, indicating transient accessibility of the protein pocket that makes intramolecular contact with the tripeptide. Therefore, the results here supported the targeting of the protein's C-terminus as an effective strategy for inhibitor design, with the binding pocket of the tripeptide predicted to be druggable.

3.3. Compound design, screening, selection, and demonstration of specificity for poxvirus

Given that ^{215}GFI^{217} is an important sequence within the C-terminus of D4, the ideal inhibitors, therefore, must contain properties comparable to this tripeptide. As an initial approach, we investigated the ability of various peptides of the C-terminus up to seven-amino acids long (^{212}WAQGFIY^{218}) to inhibit *in vitro* processive DNA synthesis.

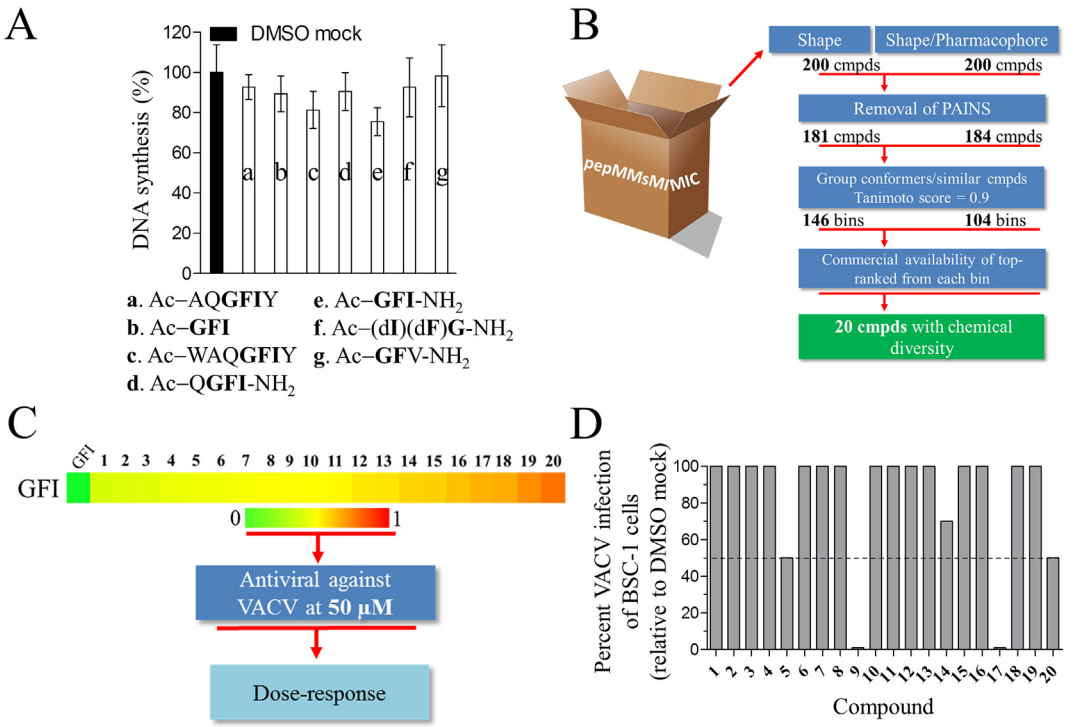

Fig. 3. FC-6407 is identified from virtual screening. (A) Peptides corresponding to the C-terminus of D4 were designed and tested for the ability to inhibit *in vitro* DNA synthesis at a single-dose of 500 µM. (B) Schematic diagram depicting the virtual screening procedure used to select commercially available small molecule mimics of the ^{215}GFI^{217} tripeptide and subsequent identification of the chemically diverse compounds. (C,D) Diversity is defined by the compounds' Tanimoto coefficients (Tc) and ordered by 1-Tc to depict compounds most to least similar to the GFI motif. The compounds were screened at a single dose of 50 µM for their ability to inhibit VACV infection of BSC-1 cells. Only compounds showing ≥50% activity were subjected to dose-response studies in both the plaque reduction assay and *in vitro* processive DNA synthesis. Compound **9** is designated as FC-6407.

When treated at a single dose of 500 µM, no significant inhibition was observed (Fig. 3A). Since short peptides tend to lack structure, the absence (or minimal gain) of activity was likely due to no (or negligible) gain in the binding enthalpy required to compensate for the entropic loss. Therefore, we investigated small molecule mimics of ^{215}GFI^{217}, with the hope that these small molecules would be endowed with intrinsic rigidity. To this end, a virtual search for compounds that explored the 3-dimensional chemical space of ^{215}GFI^{217} was performed with the web-based pepMMsMIMIC (Floris et al., 2011). From a search of nearly four million commercially-available compounds (which corresponded to approximately 17 million conformers), 20 chemically-diverse compounds were chosen on the basis of shape and shape/pharmacophore similarities (Fig. 3 and Supplementary Fig. S2).

Of the 20 compounds, four showed the ability to inhibit VACV infection of BSC-1 cells (Fig. 3D). However, only thiophene **9** (designated as FC-6407) also effectively blocked processive DNA synthesis and was therefore pursued (Supplementary Table S2 and Fig. 4B). FC-6407 showed the ability to specifically inhibit the infection of BSC-1 cells by a panel of orthopoxviruses consisting of VACV, cowpox virus (CPXV), and rabbitpox virus (RPXV) with EC_{50} values of 19.7, 8.4, and 18.7 µM, respectively, but not the unrelated DNA virus, herpes simplex virus (HSV-1) (Fig. 3A). Importantly, the antiviral activity was distinct from cytotoxicity, as minimal toxicity was observed at 100 µM compound after 24-h treatment and an estimated CC_{50} value of 31.7 µM only when extended to 72 h (Supplementary Table S2). Since the effective inhibition of viral plaque formation was readily achieved well within 24 h, the observed cytotoxicity after extended exposure may need to be addressed in future optimization. Consistently, FC-6407 effectively blocked *in vitro* DNA synthesis comprised of VACV proteins (IC_{50} = 13.4 µM; Fig. 3B) without demonstrable promiscuous DNA-binding (Fig. 4C). In accordance with the lack of antiviral activity against HSV-1 infection (Fig. 4A), FC-6407 did not block HSV-1 DNA synthesis (Fig. 4B).

3.4. D4 is a target of FC-6407

Three orthogonal methods were investigated to assess the binding of FC-6407 to D4: differential scanning fluorimetry (DSF), surface plasmon resonance (SPR), and DARTS.

For DSF studies, D4 was incubated with increasing compound concentrations. As shown in Fig. 5A and Table 1, a dose-dependent decrease in thermal shift was observed (ΔT_m = −0.86 and −1.55 for 25 and 50 µM treatments, respectively). Because a negative thermal shift can be due to ligand-binding to the unfolded/denatured protein state (Cimmperman et al., 2008), it therefore implicates the binding of FC-6407 to a conformationally unfolded subpopulation (or protein region) of D4. Indeed, this is consistent with the observed increase in temperature-sensitivity of D4 proteins when perturbed at the C-terminus compared to the N-terminus (Nuth et al., 2016) and suggests D4 as conformationally heterogeneous. By comparison, the drugs cidofovir (CDV) and tecovirimat, both known inhibitors of different poxviruses (De Clercq, 2002; Duraffour et al., 2010), displayed no thermal shifts (within experimental errors) up to 50 µM concentrations (Table 1).

Compound-binding was next examined by SPR. Using an NTA senor chip, His-tagged D4 was captured onto the Ni-charged active flow cell and crosslinked, while His-tagged MBP was similarly prepared for the reference flow cell to serve as a matching and unrelated protein surface. A dose-response was observed for FC-6407, yielding a binding affinity K_D = 22.8 µM as estimated by steady-state analysis (Fig. 5B), a value that approximated the anti-processivity value (IC_{50} = 13.4 µM). By comparison, near- or below-baseline signals for up to 50 µM compound and a lack of dose-response were observed for both CDV and tecovirimat, with CDV showing slight binding to the active flow cell at 25 and 50 µM concentrations, reflecting nonspecific binding at the higher

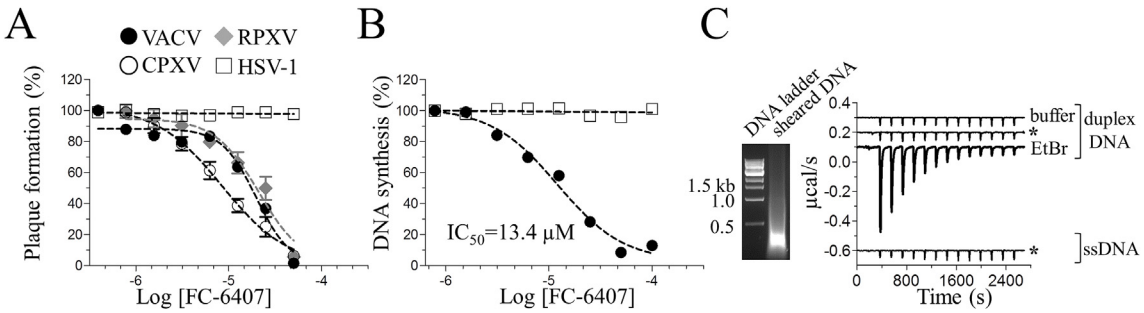

Fig. 4. FC-6407 possesses antiviral and anti-processivity activities against poxviruses. (A) FC-6407 effectively inhibits orthopoxvirus members VACV, CPXV, and RPXV with extracted EC_{50} values of 19.7, 8.4, and 18.7 µM, respectively. No dose-response is observed against HSV-1. Shown are averages of n = 2–5 replicates, with standard deviations shown for n > 2. (B) *In vitro* processive DNA synthesis was performed by combining viral DNA polymerase (UL30 for HSV-1; E9 polymerase for VACV) with their respective processivity factor (UL42 for HSV-1; D4 and A20 for VACV). (C) DNA-binding assessment by isothermal titration calorimetry (ITC). Heat traces are shown with the use of random duplex DNA (sheared DNA, shown resolved on 1% agarose gel) or single-stranded DNA (ssDNA) with the use of d(TC) 15-mer. Heat traces are rescaled to permit comparison and are shown without further deconvolution. The lack of DNA-binding by FC-6407 is demonstrated by heat traces (asterisks) equivalent to the heats of dilution generated by the buffer injections alone. By comparison, appreciable heats and saturating signals are observed for the binding of ethidium bromide (EtBr) to duplex DNA.

concentrations (Fig. 5B).

Finally, compound-binding was investigated by DARTS by incubating increasing concentrations of test compounds with crude bacterial cell lysates expressing recombinant D4 or control proteins. Since the binding of a compound disrupts the proteolytic degradation of the intended target (Lomenick et al., 2009), the observed increase in D4 protein levels, in comparison to the mock treatment, supported D4 as the protein target of FC-6407 (Fig. 4C). By contrast, no dose-response was observed when FC-6407 was incubated with MBP, MBP-$A20_{63}$, or MBP-hERβ-N (Fig. 5C). Finally, neither CDV nor tecovirimat produced a dose-response against D4 (Fig. 5D), further validating D4 as the protein target of FC-6407.

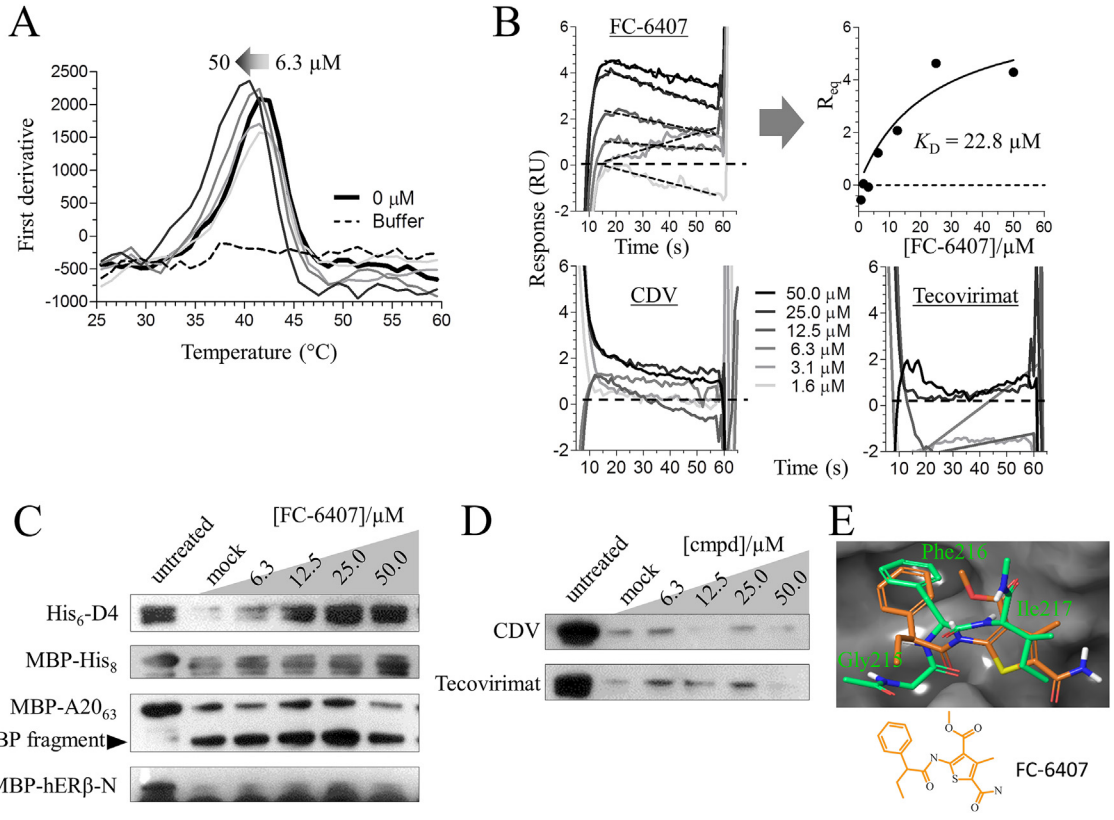

Fig. 5. Target validation of compound FC-6407 is assessed by DSF (A), SPR (B), and DARTS (C,D). (A) Shown is the dose-response generated after the incubation of D4 with increasing concentrations of FC-6407. (B) For SPR, the sensor chip NTA was crosslinked with MBP onto the reference flow cell and D4 onto the active flow cell. R_{eq} is the response from steady-state, shown as dashed lines in the sensogram overlay and CDV = cidofovir. The estimated affinity for binding of FC-6407 is shown. (C) FC-6407 shows a dose-dependent proteolytic protection of D4 proteins, but not to unrelated proteins. FC-6407 was incubated with diluted crude lysates expressing the indicated proteins, and proteolysis was achieved by the addition of Pronase at 1:37.5 dilution for the determination of MBP, 1:150 for $A20_{63}$, 1:300 for D4, and 1:2400 for hERβ-N. Protein binding is reflected by the increase in detected protein levels in comparison to the mock treatment. (D) D4 shows a lack of dose-response from poxvirus drugs. (E) The docked pose of FC-6407 (orange) is shown superimposed onto the ^{215}GFI^{217} motif of D4 (green) to allow insights into the positioning of the compound.

Table 1
Summary of DSF experiments at 25 and 50 μM compound treatments.

	ΔT_m (°C)
Compound	25, 50 μM
FC-6407	−0.86 ± 0.43, −1.55 ± 0.16
CDV	−0.37 ± 0.14, −0.27 ± 0.37
Tecovirimat	−0.37 ± 0.08, −0.26 ± 0.10

T_m = 42.24 ± 0.66 °C for D4. Values for FC-6407 reflect n = 9 and n = 3 for cidofovir (CDV) and tecovirimat.

4. Discussion

As a category A infectious agent, there is a need for the development of therapeutics against smallpox. Tecovirimat is a recently approved drug that effectively inhibits egress in orthopoxviruses by targeting the viral F13 phospholipase (Bailey et al., 2007; Yang et al., 2005). However, a concern with single-agent therapy is the potential to develop drug resistance. Therefore, the discovery of novel therapeutics with different targets could contribute to curbing the potential appearance of virus mutants. For example, from a group of 13 patients with another large DNA virus, CDV-resistance was observed in 29% of patients after three months of treatment for cytomegalovirus retinitis (Jabs et al., 1998).

The processivity factor D4 represents a compelling therapeutic target. Since processivity factors recognize their cognate DNA polymerases, the targeting of D4 is speculated to be specific to poxviruses. Moreover, processivity factors are essential for DNA replication and virus viability (Millns et al., 1994; Stuart et al., 1993), and there is a necessity for fidelity in order to maintain a functional protein. Therefore, it is reasonable to speculate that the D4R gene would be less prone to mutations. A prediction of protein disorder identified five regions spanning the D4 protein, with parts of these regions comprising interfaces for A20−D4 and D4−D4 interactions (Nuth et al., 2016). These disordered regions may reflect important dynamics that are key drivers for promoting the formation of the dimeric A20−D4 or D4−D4 complex. Given that the binding of a ligand can impact protein function through modulation of dynamics (Gibbs, 2014), an inhibitor that would disrupt dynamics on D4 was sought. While more details are needed to understand the role of the dynamics through experiments such as NMR relaxation studies and longer MD simulations, the production of insoluble and nonfunctional proteins through perturbation of the C-terminal ^{215}GFI^{217} motif through mutagenesis (Nuth et al., 2016) and the loss of soluble proteins upon conjugation with maleimide dyes (Fig. 2A) implicate the disruption of this dynamics as likely energetically unfavorable and could lead to protein misfolding. Indeed, ^{215}GFI^{217} overlaps one of these disorder regions and is speculated to anchor the C-terminus through intramolecular contacts (Fig. 2C). Therefore, the displacement of ^{215}GFI^{217} is speculated to be an effective strategy for perturbing the dynamics.

FC-6407 is demonstrated to be specific for D4. Molecular docking of FC-6407 onto D4 predicts a reasonable superimposition of FC-6407 onto ^{215}GFI^{217}, with the potential constraint/rigidity likely afforded by the thiophene moiety positioned along Ile^{217} (Fig. 5E). Since compound rigidity is important for achieving the correct binding mode for target engagement (Lawson et al., 2018), this is in line with the lack of activities observed by the peptide mimics (Fig. 3A).

5. Conclusions

Exploiting the requirement of the ^{215}GFI^{217} motif for protein function, a novel small molecule mimic has been identified for future optimization efforts. Since ^{215}GFI^{217} is conserved among orthopoxviruses, FC-6407 is a promising scaffold as a broad inhibitor of poxviruses.

Declarations of interest

None.

Acknowledgments

Funding: This work was supported by the National Institutes of Health [grant number SBIR-1R44AI115759]. The funders had no role in the study design, in the collection, analysis, and interpretation of data, in the writing of the report, or in the decision to submit the article for publication. The authors thank Dr. Thomas R. Bailey for his insights.

Appendix A. Supplementary data

Supplementary data to this article can be found online at https://doi.org/10.1016/j.antiviral.2018.12.011.

References

Aguado, B., Selmes, I.P., Smith, G.L., 1992. Nucleotide sequence of 21.8 kbp of variola major virus strain Harvey and comparison with vaccinia virus. J. Gen. Virol. 73 (Pt 11), 2887–2902.
Baell, J.B., Holloway, G.A., 2010. New substructure filters for removal of pan assay interference compounds (PAINS) from screening libraries and for their exclusion in bioassays. J. Med. Chem. 53, 2719–2740.
Bailey, T.R., Rippin, S.R., Opsitnick, E., Burns, C.J., Pevear, D.C., Collett, M.S., Rhodes, G., Tohan, S., Huggins, J.W., Baker, R.O., Kern, E.R., Keith, K.A., Dai, D., Yang, G., Hruby, D., Jordan, R., 2007. N-(3,3a,4,4a,5,5a,6,6a-Octahydro-1,3-dioxo-4,6- ethenocycloprop[f]isoindol-2-(1H)-yl)carboxamides: identification of novel orthopoxvirus egress inhibitors. J. Med. Chem. 50, 1442–1444.
Boyle, K.A., Stanitsa, E.S., Greseth, M.D., Lindgren, J.K., Traktman, P., 2011. Evaluation of the role of the vaccinia virus uracil DNA glycosylase and A20 proteins as intrinsic components of the DNA polymerase holoenzyme. J. Biol. Chem. 286, 24702–24713.
Cimmperman, P., Baranauskiene, L., Jachimoviciute, S., Jachno, J., Torresan, J., Michailoviene, V., Matuliene, J., Sereikaite, J., Bumelis, V., Matulis, D., 2008. A quantitative model of thermal stabilization and destabilization of proteins by ligands. Biophys. J. 95, 3222–3231.
Ciustea, M., Silverman, J.E., Druck Shudofsky, A.M., Ricciardi, R.P., 2008. Identification of non-nucleoside DNA synthesis inhibitors of vaccinia virus by high-throughput screening. J. Med. Chem. 51, 6563–6570.
Cowgill, R.W., 1970. Fluorescence and protein structure. XVII. On the mechanism of peptide quenching. Biochim. Biophys. Acta 200, 18–25.
Czarnecki, M.W., Traktman, P., 2017. The vaccinia virus DNA polymerase and its processivity factor. Virus Res. 234, 193–206.
Dabrowski, P.W., Radonic, A., Kurth, A., Nitsche, A., 2013. Genome-wide comparison of cowpox viruses reveals a new clade related to Variola virus. PLoS One 8, e79953.
De Clercq, E., 2002. Cidofovir in the treatment of poxvirus infections. Antivir. Res. 55, 1–13.
Druck Shudofsky, A.M., Silverman, J.E., Chattopadhyay, D., Ricciardi, R.P., 2010. Vaccinia virus D4 mutants defective in processive DNA synthesis retain binding to A20 and DNA. J. Virol. 84, 12325–12335.
Duraffour, S., Andrei, G., Snoeck, R., 2010. Tecovirimat, a p37 envelope protein inhibitor for the treatment of smallpox infection. IDrugs 13, 181–191.
Ellison, V., Stillman, B., 2001. Opening of the clamp: an intimate view of an ATP-driven biological machine. Cell 106, 655–660.
Fenner, F., Henderson, D.A., Arita, I., Jezek, Z., Ladnyi, I.D., 1988. Smallpox and its Eradication. World Health Organization, Geneva.
Floris, M., Masciocchi, J., Fanton, M., Moro, S., 2011. Swimming into peptidomimetic chemical space using pepMMsMIMIC. Nucleic Acids Res. 39, W261–W269.
Gibbs, A.C., 2014. Elements and modulation of functional dynamics. J. Med. Chem. 57, 7819–7837.
Grosenbach, D.W., Honeychurch, K., Rose, E.A., Chinsangaram, J., Frimm, A., Maiti, B., Lovejoy, C., Meara, I., Long, P., Hruby, D.E., 2018. Oral tecovirimat for the treatment of smallpox. N. Engl. J. Med. 379, 44–53.
Gubser, C., Hue, S., Kellam, P., Smith, G.L., 2004. Poxvirus genomes: a phylogenetic analysis. J. Gen. Virol. 85, 105–117.
Hornak, V., Abel, R., Okur, A., Strockbine, B., Roitberg, A., Simmerling, C., 2006. Comparison of multiple Amber force fields and development of improved protein backbone parameters. Proteins 65, 712–725.
Jabs, D.A., Enger, C., Forman, M., Dunn, J.P., 1998. Incidence of foscarnet resistance and cidofovir resistance in patients treated for cytomegalovirus retinitis. The cytomegalovirus retinitis and viral resistance study group. Antimicrob. Agents Chemother. 42, 2240–2244.
Lawson, A.D.G., MacCoss, M., Heer, J.P., 2018. Importance of rigidity in designing small molecule drugs to tackle protein-protein interactions (PPIs) through stabilization of desired conformers. J. Med. Chem. 61, 4283–4289.
Lomenick, B., Hao, R., Jonai, N., Chin, R.M., Aghajan, M., Warburton, S., Wang, J., Wu, R.P., Gomez, F., Loo, J.A., Wohlschlegel, J.A., Vondriska, T.M., Pelletier, J., Herschman, H.R., Clardy, J., Clarke, C.F., Huang, J., 2009. Target identification using drug affinity responsive target stability (DARTS). Proc. Natl. Acad. Sci. U.S.A. 106,

21984–21989.
Longini Jr., I.M., Halloran, M.E., Nizam, A., Yang, Y., Xu, S., Burke, D.S., Cummings, D.A., Epstein, J.M., 2007. Containing a large bioterrorist smallpox attack: a computer simulation approach. Int. J. Infect. Dis. 11, 98–108.
Millns, A.K., Carpenter, M.S., DeLange, A.M., 1994. The vaccinia virus-encoded uracil DNA glycosylase has an essential role in viral DNA replication. Virology 198, 504–513.
Muino, P.L., Callis, P.R., 2009. Solvent effects on the fluorescence quenching of tryptophan by amides via electron transfer. Experimental and computational studies. J. Phys. Chem. B 113, 2572–2577.
Nuth, M., Guan, H., Ricciardi, R.P., 2016. A conserved tripeptide sequence at the C terminus of the poxvirus DNA processivity factor D4 is essential for protein integrity and function. J. Biol. Chem. 291, 27087–27097.
Nuth, M., Guan, H., Zhukovskaya, N., Saw, Y.L., Ricciardi, R.P., 2013. Design of potent poxvirus inhibitors of the heterodimeric processivity factor required for viral replication. J. Med. Chem. 56, 3235–3246.
Nuth, M., Huang, L., Saw, Y.L., Schormann, N., Chattopadhyay, D., Ricciardi, R.P., 2011. Identification of inhibitors that block vaccinia virus infection by targeting the DNA synthesis processivity factor D4. J. Med. Chem. 54, 3260–3267.
Pettersen, E.F., Goddard, T.D., Huang, C.C., Couch, G.S., Greenblatt, D.M., Meng, E.C., Ferrin, T.E., 2004. UCSF Chimera–a visualization system for exploratory research and analysis. J. Comput. Chem. 25, 1605–1612.
Pronk, S., Pall, S., Schulz, R., Larsson, P., Bjelkmar, P., Apostolov, R., Shirts, M.R., Smith, J.C., Kasson, P.M., van der Spoel, D., Hess, B., Lindahl, E., 2013. GROMACS 4.5: a high-throughput and highly parallel open source molecular simulation toolkit. Bioinformatics 29, 845–854.
Ricciardi, R.P., Lin, K., Chen, X., Dorjsuren, D., Shoemaker, R., Sei, S., 2005. Rapid screening of chemical inhibitors that block processive DNA synthesis of herpesviruses: potential application to high-throughput screening. Methods Mol. Biol. 292, 481–492.
Sastry, G.M., Adzhigirey, M., Day, T., Annabhimoju, R., Sherman, W., 2013. Protein and ligand preparation: parameters, protocols, and influence on virtual screening enrichments. J. Comput. Aided Mol. Des. 27, 221–234.
Schormann, N., Sommers, C.I., Prichard, M.N., Keith, K.A., Noah, J.W., Nuth, M., Ricciardi, R.P., Chattopadhyay, D., 2011. Identification of protein-protein interaction inhibitors targeting vaccinia virus processivity factor for development of antiviral agents. Antimicrob. Agents Chemother. 55, 5054–5062.
Silverman, J.E., Ciustea, M., Shudofsky, A.M., Bender, F., Shoemaker, R.H., Ricciardi, R.P., 2008. Identification of polymerase and processivity inhibitors of vaccinia DNA synthesis using a stepwise screening approach. Antivir. Res. 80, 114–123.
Stanitsa, E.S., Arps, L., Traktman, P., 2006. Vaccinia virus uracil DNA glycosylase interacts with the A20 protein to form a heterodimeric processivity factor for the viral DNA polymerase. J. Biol. Chem. 281, 3439–3451.
Stuart, D.T., Upton, C., Higman, M.A., Niles, E.G., McFadden, G., 1993. A poxvirus-encoded uracil DNA glycosylase is essential for virus viability. J. Virol. 67, 2503–2512.
Upton, C., Stuart, D.T., McFadden, G., 1993. Identification of a poxvirus gene encoding a uracil DNA glycosylase. Proc. Natl. Acad. Sci. U.S.A. 90, 4518–4522.
Warnmark, A., Wikstrom, A., Wright, A.P., Gustafsson, J.A., Hard, T., 2001. The N-terminal regions of estrogen receptor alpha and beta are unstructured in vitro and show different TBP binding properties. J. Biol. Chem. 276, 45939–45944.
Wright, P.E., Dyson, H.J., 1999. Intrinsically unstructured proteins: re-assessing the protein structure-function paradigm. J. Mol. Biol. 293, 321–331.
Yang, G., Pevear, D.C., Davies, M.H., Collett, M.S., Bailey, T., Rippen, S., Barone, L., Burns, C., Rhodes, G., Tohan, S., Huggins, J.W., Baker, R.O., Buller, R.L., Touchette, E., Waller, K., Schriewer, J., Neyts, J., DeClercq, E., Jones, K., Hruby, D., Jordan, R., 2005. An orally bioavailable antipoxvirus compound (ST-246) inhibits extracellular virus formation and protects mice from lethal orthopoxvirus challenge. J. Virol. 79, 13139–13149.